Korean J. Chem. Eng., 36(4), 605-612 (2019)
DOI: 10.1007/s11814-019-0241-y

pISSN: 0256-1115
eISSN: 1975-7220

Fabrication of magnetically recyclable ZrO_2-TiO_2/$CoFe_2O_4$ hollow core/shell photocatalysts: Improving photocatalytic efficiency under sunlight irradiation

Hong-xia Jing†, Jing Huang, Na Li, Long-xiang Li, and Jingyue Zhang

Department of Chemistry, School of Science, North University of China, Taiyuan 030051, China
(*Received 26 November 2018 • accepted 11 February 2019*)

Abstract−TiO_2 is an important material for photocatalytic oxidation to degrade organic pollutants, but its utilization under visible light is low, recovery is difficult, and stability is poor. We prepared ZrO_2-TiO_2/$CoFe_2O_4$ (Zr-Ti/Co) photocatalyst with hollow core-shell structure by sol-gel method and layer-by-layer self-assembly method with tetrabutyl titanate and Zirconium n-butoxide as main raw materials. The samples were characterized and analyzed by X-ray diffraction (XRD), transmission electron microscopy (TEM), solid ultraviolet visible diffuse reflection (UV-Vis DRS), fluorescence (FL), ultraviolet visible absorption (UV), vibrating sample magnetometer (VSM). It is concluded that the TiO_2 maintains a good anatase phase structure in the Zr-Ti-Co photocatalyst. Under UV light and sunlight, the degradation rate of the photocatalyst reached 96.1% and 99.7% for 60 min, respectively, for Rhodamine B (10 mg/L) reaction system. And after repeated use for five times, it still showed better regeneration and reuse.

Keywords: Photocatalytic Performance, ZrO_2-TiO_2/$CoFe_2O_4$ Photocatalyst, Sunlight, Regeneration and Reuse

INTRODUCTION

For the problem of environmental pollution, how to quickly and easily control a variety of organic pollutants and conform to the concept of green sustainable development has become an area that people are constantly exploring [1,2]. Photocatalytic oxidation technology [3,4] has great application potential in wastewater treatment. The most common semiconductor catalytic material is TiO_2, which has attracted extensive attention for its good photocatalytic performance. Although TiO_2 nanomaterials have the advantages of high specific surface area, non-selective degradation, are available at room temperature and pressure, non-toxic, with chemical and biological inertness, high photochemical stability and low price [5-7]. However, the forbidden band width of anatase TiO_2 is 3.20 eV, so its solar utilization is limited [8]. The difficulty of separation from the reaction system limits the industrial development in photocatalysis [9,10].

The radius of titanium ions and zirconium ions is 60.5 pm and 72 pm, respectively. Because of their small difference in ionic radius, zirconium-modified titanium dioxide can be used to induce nano-TiO_2 lattice distortion to form an electron trap, thereby achieving the purpose of separating electron holes [11-13]. Moreover, since TiO_2 (3.2 eV) has a narrower band gap than ZrO_2 (5 eV), and the conduction band position of TiO_2 is higher than that of ZrO_2, photoinduced conduction band electrons can be injected into the ZrO_2 conduction band to generate effective electron holes [14-16]. Therefore, the ZrO_2 doped modified TiO_2 can increase the quantum efficiency and improve the photocatalytic efficiency of the TiO_2 [17-20].

$CoFe_2O_4$ has high magnetocrystalline anisotropy, high coercive force and magnetic saturation strength, and stable chemical properties [21,22]. The magnetic photocatalyst can be prepared by using $CoFe_2O_4$ as the magnetic core to improve the magnetic recyclability of the photocatalyst. Gao [23] showed that the removal rate of Cr (VI) by $CoFe_2O_4$/TiO_2 was 13% lower than that of TiO_2 after 180 min. Because of the strong absorbance and darkening of the magnetic core in the visible light region and the ultraviolet light region, the defect of the light transmittance of the system is deteriorated [24], which tends to cause a decrease in photocatalytic activity. Laohhasurayotin [25] research shows that the 20 nm SiO_2 interlayer can effectively inhibit the electron transfer induced by TiO_2 and Mn-Zn ferrite to maintain the photoactivity of the catalyst. Yang [26] research showed that the TSC sample showed the best photocatalytic activity when the Si/Co molar ratio was 28. Because coating the SiO_2 inert isolation layer on the magnetic core can avoid an electron reaction, photolysis reaction, and absorption of the magnetic core, and prevent the magnetic core from being oxidized during the heat treatment [27,28]. The magnetic suspension-loaded photocatalyst has the characteristics of high specific surface area and high mass transfer efficiency of the suspension phase photocatalyst, and it can be recovered and reused by using the magnetic property, which overcomes the shortcoming of the recovery of the suspended TiO_2 powder [29-32].

If the SiO_2 coating of the composite material is etched, it is possible to prepare a composite material having a hollow structure, which can increase the specific surface area of the photocatalyst and prevent photolysis of the magnetic core. Therefore, the photocatalytic performance and the reusability of photocatalyst can be further improved. In this study, a new photocatalyst Zr-Ti/Co (SiO_2 etched) was prepared by sol-gel method and layer self-assembly method, using tetrabutyl titanate, zirconium n-butoxide as the main raw material. The photocatalytic properties of photocatalyst were

†To whom correspondence should be addressed.
E-mail: jhx820215@126.com

studied under ultraviolet light and sunlight.

EXPERIMENTAL

1. Chemicals

Tetrabutyl titanate, tetraethyl orthosilicate, cobalt nitrate (analytical grade, Sinopharm Chemical Reagent Co., Ltd.); zirconium n-butoxide (analytical grade, Kunming Yinlong Chemical Co., Ltd.); ferric nitrate (analytical grade, Tianjin Fuchen Chemical Reagent Factory); citric acid, glacial acetic acid, sodium hydroxide (analytically pure, Da Mao Chemical Reagent Co., Ltd.); ahydrous ethanol (analytically pure, Sailboat Chemical Reagent Co., Ltd.); rhodamine B (analytical grade, Beijing Chemical Plant); the above reagents were not treated before use.

2. Preparation

Preparation of TiO_2 photocatalyst. First, 10.0 ml of tetrabutyl titanate was slowly added to 30.0 ml of absolute ethanol, and ultrasonically mixed to form a yellow clear solution A. Solution B was mixed by deionized water 10.0 ml, glacial acetic acid 15.0 ml and anhydrous ethanol 10.0 ml. Solution A was vigorously stirred in 25 °C constant temperature water bath, then solution B was added dropwise to solution A until it was added dropwise completed, and the mixture was stirred until the sol state. After aging for 24 h at room temperature, it was dried in a constant temperature oven at 60 °C for 12 h, calcined at 600 °C for 2 h, and naturally cooled to room temperature. After grinding for half an hour, a pure TiO_2 photocatalyst was obtained. The Zr-Ti photocatalyst was synthesized in the same manner by adding n-butoxyzirconium (m_{ZrO2} : m_{TiO2}=1 : 14) to form the solution A.

Preparation of Zr-Ti/Si/Co photocatalyst. Spinel cobalt ferrite $CoFe_2O_4$ was synthesized by sol-gel self-propagating combustion method. The 0.05 g $CoFe_2O_4$ powder was dispersed in a mixed solution of 100 ml of absolute ethanol, 25 ml of deionized water and 3.5 ml of ammonia water and stirred by supersonic for 10 min. It was vigorously stirred in 45 °C constant temperature water bath, and 0.4 ml of tetraethyl silicate solution (Si : Co molar ratio of 28 : 1) [26] was slowly added dropwise. After stirring for 24 h, it was washed alternately with absolute ethanol and deionized water. The SiO_2/$CoFe_2O_4$ (Si/Co) composite material was obtained by drying. The 0.45 g Si/Co composite was dispersed in 150 ml of Zirconium n-butoxide anhydrous ethanol solution (m_{ZrO2} : m_{TiO2}=1 : 14). It was vigorously stirred in 45 °C constant temperature water bath, and 4.0 ml of concentrated ammonia water and 6.0 ml of tetrabutyl titanate (Ti : Co molar ratio 50 : 1) was slowly added dropwise. After stirring for 24 h, it was dried, calcined, and ground. Then the Zr-Ti/Si/Co photocatalyst was obtained.

Preparation of Zr-Ti/Co photocatalyst. The 1.0 g Zr-Ti/Si/Co composite was dispersed in 100 ml 0.5 mol/L NaOH solution [33]. It was stirred in 80 °C constant temperature water bath for 4 h. Then it was centrifuged, washed, dried at 60 °C for 12 h, calcined at 600 °C for 2 h, natural cooled to room temperature and ground 0.5 h. Then the Zr-Ti/Co photocatalyst was obtained.

3. Photocatalytic Experiments

On the basis of experiments and correlated references, 50.0 mg photocatalyst was added to 50.0 ml 10.0 mg/L rhodamine B solution in a beaker. When the mixed solution achieved adsorption equilibrium by ultrasonic for 30 min, it was poured into an ultraviolet light reactor, which was 15 cm distant from the mercury lamp. A sample of 3.0 ml was sampled in a centrifuge tube at intervals of 15 min or 10 min. After centrifugation, its clear liquid was taken. The absorbance of the clear liquid was measured by an ultraviolet-visible spectrophotometer at 554 nm. At last a degradation curve was drawn.

The photocatalytic reaction was carried out in the same way under sunlight (sunlight at noon in mid-May, Taiyuan, Shanxi Province, China, temperature was about 25 °C), and a degradation curve was drawn.

4. Characterization

The crystal structure of the prepared sample was analyzed by Cu-Ka radiation by an X-ray diffractometer (XRD, D/max-ray, Nippon Science). The morphology was measured by a transmission electron microscope (TEM, JEM-1011, JEOL Ltd.). The photoluminescence spectrum was measured using a fluorescence spectrometer (FL, F-2700, Hitachi High-Tech Co., Ltd.). The chemical bonding state was evaluated by Fourier transform infrared spectroscopy (FTIR, FI-IR 4800F, Shimadzu Corporation, Japan). The magnetic properties of the samples were obtained using a multi-vibration sample magnetometer (VSM, VSM-7307, Lake Shore). The ultraviolet visible diffuse reflectance spectrum was measured using an ultraviolet-visible diffuse reflectometer (UV-vis, UV-2600, Shimadzu Corp., Japan). The absorption spectrum curve was measured using an ultraviolet-visible spectrophotometer (UV, UV-2300, Shanghai Tianmei Instrument Co., Ltd.). The photocatalyst degradation diagram was measured using a photoreactor, which was self-made and consisted of three 15 W mercury lamps placed in parallel.

RESULTS AND DISCUSSION

1. XRD Characterization

Fig. 1 is an XRD pattern of samples. From the XRD pattern of pure TiO_2 in Fig. 1(a), it can be seen that the 2θ values are 25.23°(101), 37.72°(004), 48.08°(200), 54.03°(105), 54.98°(211), 62.66°(204),

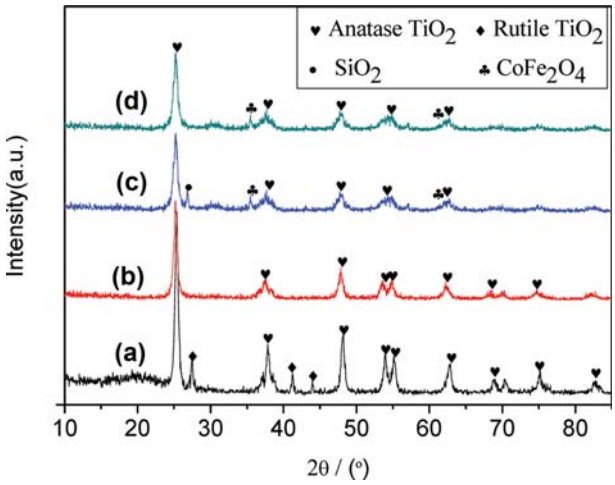

Fig. 1. XRD pattern of samples ((a) TiO_2; (b) Zr-Ti; (c) Zr-Ti/Si/Co; (d) Zr-Ti/Co).

68.80°(116), 70.34°(220), 75.14°(215), which coincide with the anatase TiO_2 (JCPDS, No. 21-1272) diffraction peak, and it can be seen that the characteristic absorption peaks appearing at 2θ values of 27.45°(110), 41.25°(111), and 43.95°(210) are consistent with rutile TiO_2 (JCPDS, No. 21-1276) diffraction peak. The peak is narrow and the intensity is high, indicating that the degree of crystallization is good. From the XRD pattern of Zr-Ti in Fig. 1(b), one does not observe the obvious ZrO_2 diffraction peak, indicating that the Zr^{4+} doping enters the TiO_2 lattice and occupies the position of Ti^{4+}, so it does not form a stable crystal form [34]. And it does not appear the absorption peak of rutile TiO_2, because the crystal transformation of TiO_2 is inhibited by Zr^{4+}. From the XRD pattern of Zr-Ti/Si/Co in Fig. 1(c), it can be seen that the characteristic absorption peaks appearing at 2θ values of 26.78°(642) and 35.60°(311) are consistent with the diffraction peaks of SiO_2 and $CoFe_2O_4$, respectively. But their strength is weak because the surface is covered with Zr-Ti outer layer, indicating that the effect of coating is good. From the XRD pattern of Zr-Ti/Co in Fig. 1(d), it can be seen that it is substantially similar to the peak shape of Fig. 1(c), except that it does not observe the diffraction peak of SiO_2. It is indicated that the SiO_2 is successfully removed by washing after being etched.

2. TEM Analysis

Fig. 2 is a TEM image of a photocatalyst. From Fig. 2(a), it can be seen that the TiO_2 nanoparticles are spherical and uniform distribution of particle size (average diameter 5-8 nm). As can be seen from Fig. 2(b), the Zr-Ti photocatalyst exhibits a ball shape with a particle size of about 10 nm, which is a little increased compared with TiO_2. Since the Zr^{4+} occupies the position of Ti^{4+}, and the ion radius of Zr^{4+} (72 pm) is larger than that of Ti^{4+} (60.5 pm). From Fig. 2(c), it can be seen that the darker color is $CoFe_2O_4$ nanoparticles, and a lighter SiO_2 coating layer can be found around it, and the outermost color is the TiO_2 coating layer. It indicates that the Zr-Ti/Si/Co core-shell nanoparticles were successfully obtained. This is based on $CoFe_2O_4$, SiO_2 is the protective layer, and TiO_2 is the shell. From Fig. 2(d), the lighter SiO_2 coating layer coated on the $CoFe_2O_4$ nanoparticles disappears. It forms a void layer with the outer layer of TiO_2 coating, indicating that the Zr-Ti/Co hollow core-shell nanoparticles are successfully obtained. It is based on $CoFe_2O_4$ as a magnetic core, hollow as a protective layer and TiO_2 as a shell. Since the SiO_2 layer is etched, the mass ratio of TiO_2 is increased at a unit mass, and the hollow structure can prevent photolysis of the core of $CoFe_2O_4$. So the hollow structure can play a protective role and reduce the electron hole recombination rate [27,28]. Therefore, the photocatalytic performance is better improved.

3. FTIR Spectroscopy

Fig. 3 is an infrared spectrum diagram of samples ((a) and (b) are Zr-Ti/Si/Co, Zr-Ti/Co, respectively). As shown in Fig. 3(a), the Zr-Ti/Si/Co photocatalyst exhibited stretching vibration of Si-O

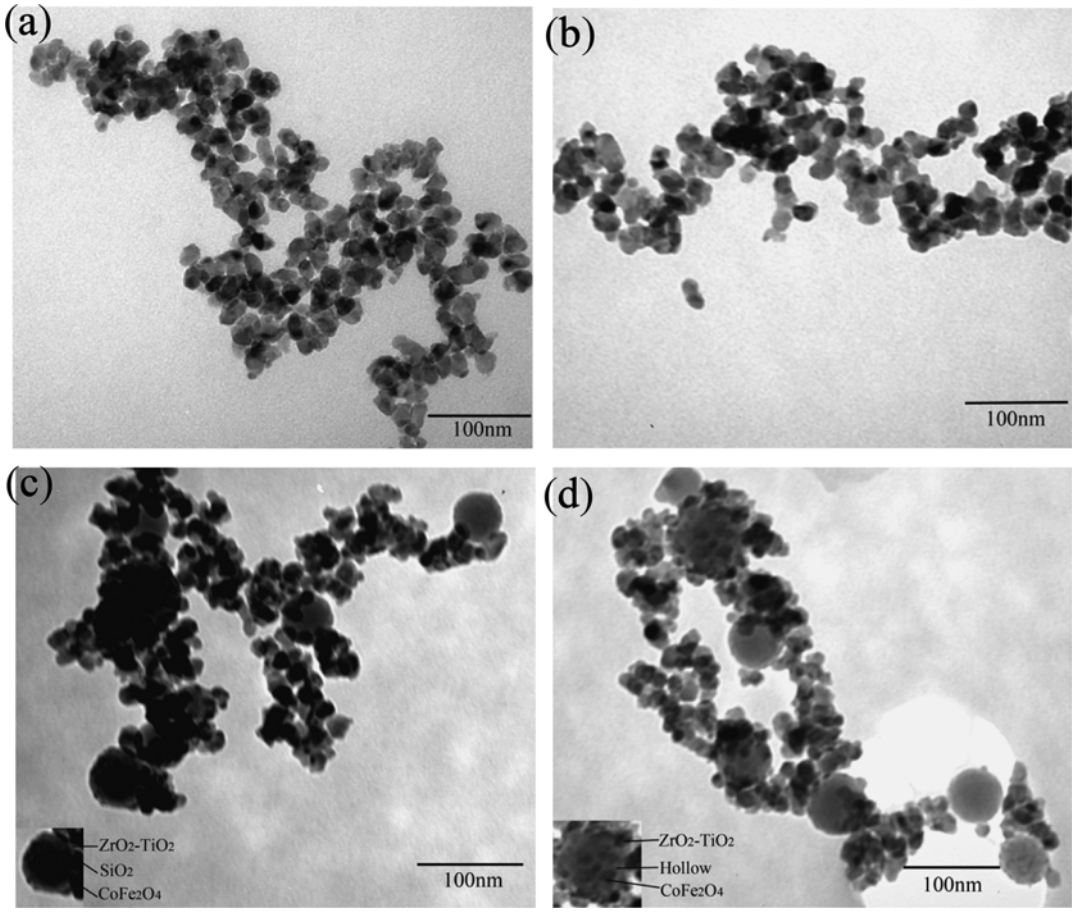

Fig. 2. TEM image of samples ((a) TiO_2; (b) Zr-Ti/Si; (c) Zr-Ti/Si/Co; (d) Zr-Ti/Co).

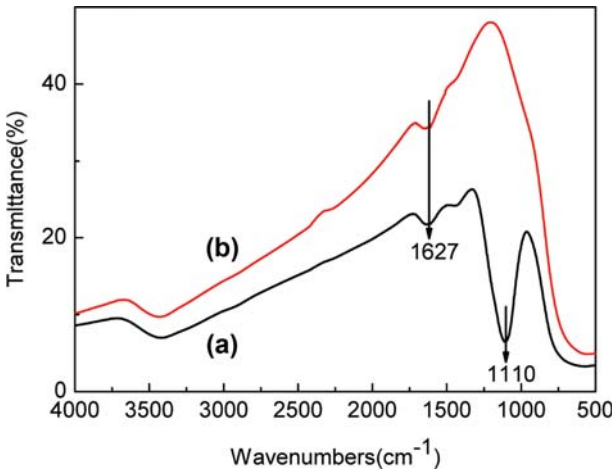

Fig. 3. FTIR spectrum of samples ((a) Zr-Ti/Si/Co; (b) Zr-Ti/Co).

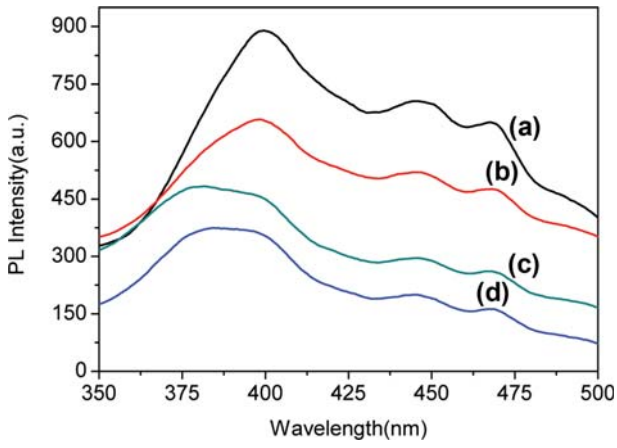

Fig. 5. Fluorescence spectrum of samples ((a) TiO_2; (b) Zr-Ti; (c) Zr-Ti/Si/Co; (d) Zr-Ti/Co).

bonds at 1,110 cm^{-1} and the stretching vibration of the H-O bonds at 1,627 cm^{-1}. After treatment with sodium hydroxide solution, the stretching vibration of the H-O bond occurred in the Zr-Ti/Co photocatalyst spectrum, but the stretching vibration of the Si-O bond did not occur as Fig. 3(b). It is indicated that the SiO_2 in the Zr-Ti/Si/Co photocatalyst reacted with the sodium hydroxide solution and generated sodium silicate solution, and the sodium silicate was successfully removed after the subsequent centrifugal washing.

4. VSM Analysis

The VSM curves of samples are shown in Fig. 4 and the magnetic parameters are listed in Table 1. From Table 1, it can be seen

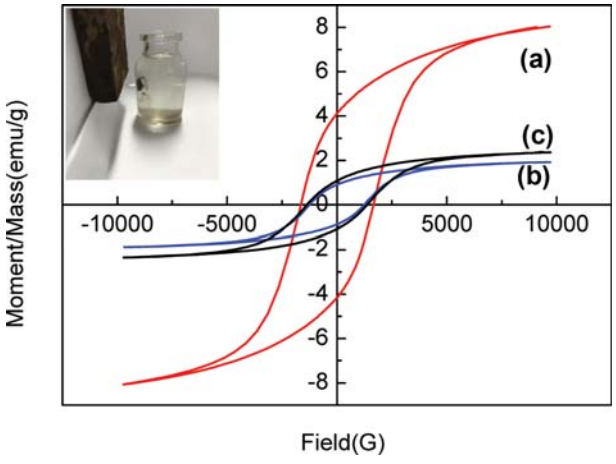

Fig. 4. VSM curve of samples ((a) Si-Co; (b) Zr-Ti/Si/Co; (c) Zr-Ti/Co).

Table 1. Magnetic parameters

Parameters / Samples	Hc/Oe	Ms/emu·g^{-1}	Mr/emu·g^{-1}
Si-Co	1656.12	8.03487	4.12354
Zr-Ti/Si/Co	1175.86	1.91463	0.90893
Zr-Ti/Co	1302.78	2.3432	1.08616

that the Si-Co photocatalyst has the highest magnetism, because the $CoFe_2O_4$, SiO_2 and TiO_2 are magnetic core, protective layer, and shell respectively, but TiO_2 and SiO_2 are non-magnetic substances [35]. The magnetism of the photocatalysts decreased with the increase as the volume of the coating. The magnetism of Zr-Ti/Co is slightly higher than that of the Zr-Ti/Si/Co photocatalyst, because the SiO_2 layer is etched. Above all, despite the decrease of magnetism compared to Si/Co, the Zr-Ti/Si/Co and Zr-Ti/Co photocatalysts can still be efficiently separated using an external magnet, which can be seen from Fig. 4 inset. The results of the VSM proved once more that the Zr-Ti/Co hollow core-shell nanoparticles are successfully obtained and have magnetic recyclable property.

5. Fluorescence Spectrum

Fig. 5 shows the photoluminescence spectra of samples, which the emission wavelength is 290 nm. TiO_2 shows absorption peaks at wavelengths of 400.0 nm, 445.0 nm, and 467.0 nm, respectively. And other samples have absorption peaks at similar positions, but the fluorescence intensity of the emission peaks is different. From the Fig. 5, the fluorescence intensity of the TiO_2, Zr-Ti, Zr-Ti/Si/Co and Zr-Ti/Co photocatalysts is sequentially decreased. The generation of the fluorescence spectrum is mainly derived from the recombination of photogenerated electron-hole pairs. When the recombination rate of photogenerated electron-hole pairs is lower, the fluorescence intensity is smaller. Due to the doping of the Zr element, a new Zr^{4+} ion is introduced into the TiO_2 lattice. Therefore, a defect is formed on the surface of the TiO_2 lattice, which can trap photogenerated electrons as a trap and improve the separation efficiency of the photogenerated carriers, so the fluorescence intensity is lowered [36-38]. Although $CoFe_2O_4$ is introduced in order to increase the recovery rate of the photocatalyst, it has a photolysis effect. The fluorescence intensity of Zr-Ti/Si/Co photocatalyst is further reduced, indicating that the SiO_2 protective layer not only prevents the negative influence of $CoFe_2O_4$ on photocatalytic performance, but also synergizes with TiO_2 to reduce the photoelectron-hole pair recombination. After the introduction and etching of the SiO_2 layer in the Zr-Ti/Co photocatalyst, the defects of the TiO_2 lattice are further increased. Therefore, the holes and electrons are effectively separated, and the recombination time is

prolonged to cause a decrease in fluorescence intensity, but also the fluorescence intensity of TiO_2, Zr-Ti, Zr-Ti/Si/Co, and Zr-Ti/Co composites is consistent with the photocatalytic activity.

6. UV-visible Diffuse Reflectance Spectroscopy

Fig. 6(A) shows the UV-visible diffuse reflectance spectrum of the sample. It can be found that the wavelength response of the TiO_2 photocatalyst is in the ultraviolet region of less than 400 nm. However, the wavelength responses of the modified Zr-Ti, Zr-Ti/Si/Co and Zr-Ti/Co photocatalysts are all red shifted to the visible region, which increases the absorption and utilization of visible light by the photocatalyst [39]. Fig. 6(B) shows the UV-visible diffuse reflection $(\alpha h\nu)^{1/2}$~Eg transformation of samples. As can be

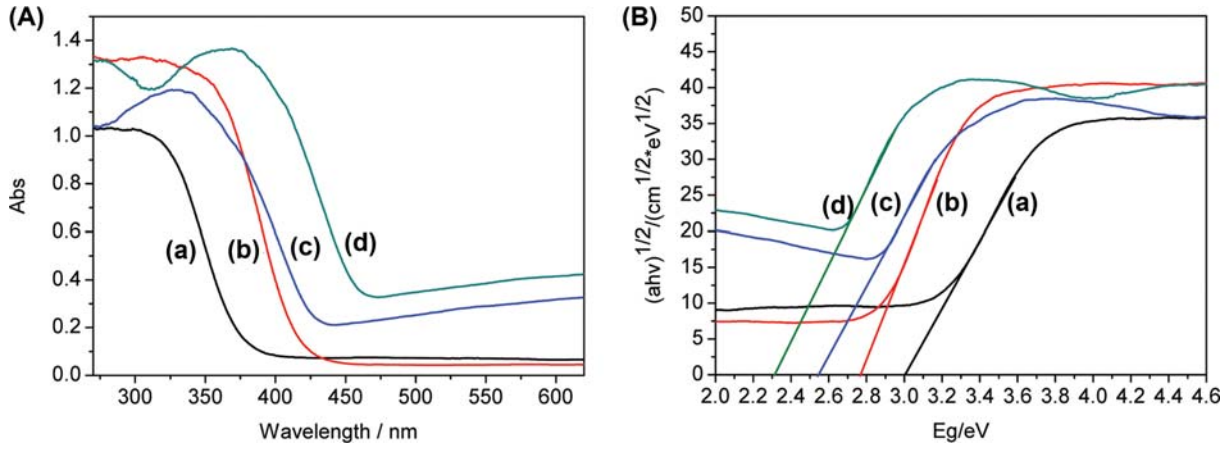

Fig. 6. (A) UV-visible diffuse reflectance spectrum; (B) the UV-visible diffuse reflection $(\alpha h\nu)^{1/2}$~Eg transformation of samples ((a) TiO_2; (b) Zr-Ti; (c) Zr-Ti/Si/Co; (d) Zr-Ti/Co).

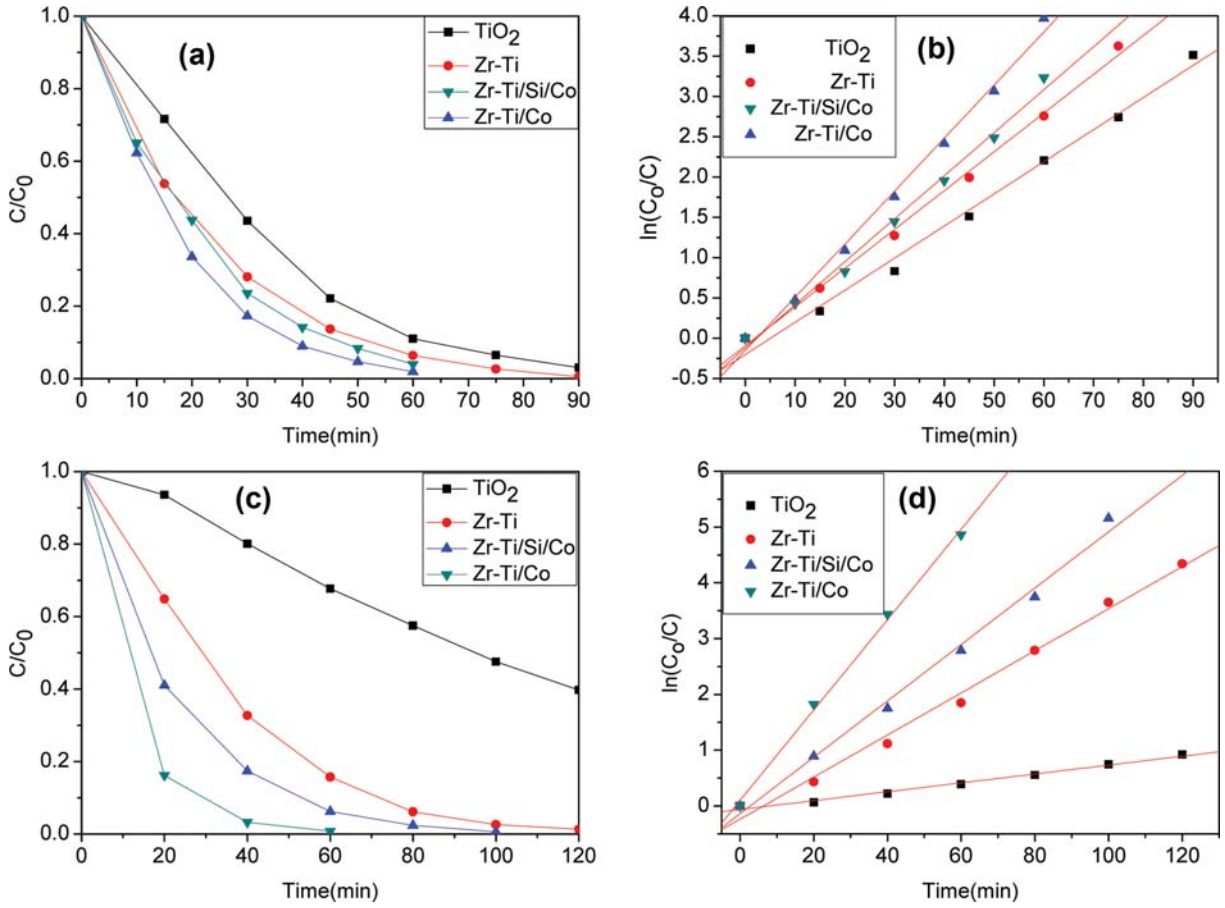

Fig. 7. Photocatalyst degradation diagram and kinetic diagram ((a) Degradation under ultraviolet light; (b) kinetic diagram under ultraviolet light; (c) degradation under sunlight; (d) kinetic diagram under sunlight).

seen, the value of the intersection of the straight line extrapolation and the abscissa according to the $(\alpha h\nu)^{1/2}$~Eg transformation diagram is the forbidden band width value of each photocatalyst. It can be concluded that the forbidden bands of TiO_2, Zr-Ti, Zr-Ti/Si/Co, and Zr-Ti/Co photocatalysts are 3.00 eV, 2.77 eV, 2.54 eV, and 2.30 eV, respectively. The smaller the forbidden band width, the smaller the energy required to generate free electrons and free holes after the valence electrons transition to the conduction band [40,41]. Moreover, the smaller band gap indicates that the photocatalyst is exhibiting a red shift, and the utilization of visible light is increased, which enhances the photocatalytic effect of the photocatalyst under visible light. Compared with TiO_2, the absorption wavelength range of other photocatalysts increases and shifts to the visible light region. The absorption wavelength of Zr-Ti/Co photocatalyst is the largest, so its photocatalytic performance under sunlight is excellent.

7. Photocatalytic Performance

Fig. 7(a) is a degradation curve of TiO_2, Zr-Ti, Zr-Ti/Si/Co, and Zr-Ti/Co photocatalysts under ultraviolet light irradiation. At 30 min, the photocatalyst degradation rates are 56.45%, 71.96%, 76.46% and 82.71%, respectively. At 60 min, the photocatalyst degradation rates are 89.00%, 93.66%, 96.06%, and 98.12%, respectively. Fig. 7(b) is a kinetic diagram of a photocatalyst under ultraviolet light irradiation and the primary kinetic parameters are listed in Table 2. The kinetics of photocatalytic degradation of rhodamine B accords with the Langmuir-Hinshelwood (L-H) kinetic model [42]. The fitting R of each photocatalyst is kept at about 0.99, indicating that the photocatalytic reaction occurs on the surface of the material, so the photocatalyst can be regenerated. It is possible to degrade the contaminants again. The k value can evaluate the catalytic ability of the photocatalyst, so the larger the k value, the better the photocatalytic effect. The k values of the TiO_2, Zr-Ti, Zr-Ti/Si/Co, and Zr-Ti/Co photocatalysts are 0.03984, 0.04811, 0.05336, and 0.06581, respectively. The results show that Zr^{4+} doped TiO_2 can effectively improve the photocatalytic effect; SiO_2 (Si : Co molar ratio of 28 : 1) is coated on $CoFe_2O_4$, which can effectively inhibit the photolysis of TiO_2 coated by magnetic core. And it can effectively improve the photocatalytic effect. Therefore, the order of the catalytic ability of each photocatalyst under ultraviolet light is: Zr-Ti/Co>Zr-Ti/Si/Co>Zr-Ti>TiO_2.

Fig. 7(c) shows the degradation curves of TiO_2, Zr-Ti, Zr-Ti/Si/Co, and Zr-Ti/Co photocatalysts under sunlight. At 60 min, the photocatalyst degradation rates are 32.28%, 84.29%, 93.83%, and 99.23%, respectively. At 120 min, the photocatalyst degradation rates are 60.28%, 98.70%, 100%, and 100%, respectively. Fig. 7(d) shows the kinetics of photocatalyst under sunlight and and the primary kinetic parameters are listed in Table 2. The kinetics of photocatalytic degradation of rhodamine B is in accordance with the Langmuir-Hinshelwood (L-H) kinetic model [42]. The fitting R of each photocatalyst is kept at around 0.99. The k values of the TiO_2, Zr-Ti, Zr-Ti/Si/Co, and Zr-Ti/Co photocatalysts are 0.00796, 0.03774, 0.05053, and 0.08101, respectively. The results show that the degradation rate of Zr-Ti/Co photocatalyst is about 10.2, 2.1 and 1.6-times higher than that of TiO_2, Zr-Ti and Zr-Ti/Si/Co photocatalysts under sunlight. Therefore, the order of the catalytic ability of each photocatalyst under sunlight is Zr-Ti/Co>Zr-Ti/Si/Co>Zr-Ti>TiO_2, which is consistent with the catalysis under ultraviolet light.

Table 2. Photocatalyst degradation kinetic parameters

		TiO_2	Zr-Ti	Zr-Ti/Si/Co	Zr-Ti/Co
UV light	k	0.03984	0.04811	0.05336	0.06581
	b	−0.2014	−0.0931	−0.1184	−0.1493
	R	0.9927	0.9909	0.9953	0.9885
Sun light	k	0.00796	0.03774	0.05053	0.08101
	b	−0.0635	−0.2380	−0.1382	−0.1001
	R	0.9864	0.9900	0.9909	0.9955

8. Renewability and Reusability Study

After completing a photocatalytic experiment, the Zr-Ti/Co photocatalyst was recovered by a magnet, washed three times with deionized water, and dried at 60 °C. The results of the photocatalytic experiment under ultraviolet light irradiation are repeated as shown in Fig. 8(a). The figure shows that the degradation rates of Zr-Ti/Co photocatalyst in the five replicate experiments are 98.12%, 96.99%, 95.61%, 94.67%, and 94.05%, respectively. Fig. 8(b) shows the kinetics of photocatalyst under ultraviolet light irradiation. The kinetics of photocatalytic degradation of rhodamine B is in accor-

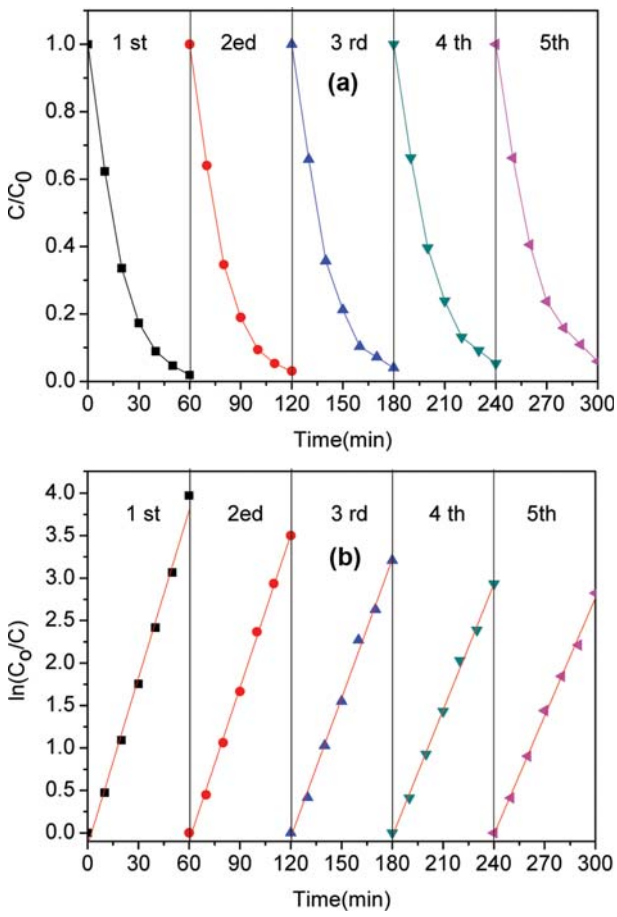

Fig. 8. Zr-Ti/Co photocatalyst repeated degradation curve and kinetic diagram.

dance with the Langmuir-Hinshelwood (L-H) kinetic model [42]. The fitting R of each photocatalyst is kept at around 0.99. The results show that the Zr-Ti/Co photocatalyst can be recovered, and the photocatalytic effect of recycling five times is only slightly reduced. This may be due to 1) the recovery of the photocatalyst by the magnet cannot achieve 100% recovery; 2) Zr-Ti/Co photocatalyst channel adsorption of a little rhodamine B is not cleaned [43]; 3) The photocatalyst was not subjected to ultrasonication when it was used again, resulting in agglomeration between the particles, so the specific surface area decreased [44]. However, Zr-Ti/Co photocatalyst still has good recyclability. The photocatalyst can be recovered in industrial process wastewater to prevent the photocatalyst from being discharged into the environment as a secondary pollutant, which reduces the cost of the photocatalyst.

SUMMARY

Zr-Ti/Co was successfully prepared by sol-gel method and layer self-assembly method. XRD analysis confirmed the coexistence of anatase TiO_2 and spinel $CoFe_2O_4$ photocatalyst. Infrared spectroscopy confirmed that the SiO_2 component was successfully etched. TEM studies showed that the Zr^{4+} doped TiO_2 layer was deposited on the Si/Co core, and the SiO_2 layer was etched to form a hollow structure. The VSM, FL and UV-Vis DRS showed that the Zr-Ti/Co photocatalyst has magnetic property, the recombination rate of photogenerated electron-hole pairs is lowest, and the absorption wavelength is red shifted to the visible region, respectively. Photocatalytic experiments showed that the degradation rate of Zr-Ti/Co photocatalyst under UV lamp and sunlight is 98.12% and 99.23% for 60 min, and it can still show better regeneration and reuse after repeated use for five times.

ACKNOWLEDGEMENT

National Natural Science Foundation of China (20871108, 51272239).

REFERENCES

1. M. Y. Xing, W. J. Xu, C. C. Dong, Y. C. Bai, J. B. Zeng, Y. Zhou, J. L. Zhang and Y. D. Yin, *Chem-US.*, **4**, 1359 (2018).
2. C. C. Dong, J. H. Ji, B. Shen, M. Y. Xing and J. L. Zhang, *Environ. Sci. Technol.*, **52**, 11297 (2018).
3. H. Z. Li, L. Y. Shen, K. F. Zhang, B. J. Sun, L. P. Ren, P. Z. Qiao, K. Pan, L. Wang and W. Zhou, *Appl. Catal. B-Environ.*, **220**, 111 (2018).
4. Z. F. Bian, J. Zhu and H. X. Li, *J. Photochem. Photobio. C.*, **28**, 72 (2016).
5. F. Han, V. S. R. Kambala, M. Srinivasan, D. Rajarathnam and R. Naidu, *Appl. Catal. A-Gen.*, **359**, 25 (2009).
6. Z. Shayegan, C. S. Lee and F. Haghighat, *Chem. Eng. J.*, **334**, 2408 (2018).
7. N. R. Khalid, A. Majid, M. B. Tahir, N. A. Niaz and S. Khalid, *Ceram. Int.*, **43**, 14552 (2017).
8. K. Sayama and H. Arakawa, *J. Cheminformatics*, **93**, 1647 (1997).
9. J. Wang, L. Peng, F. Cao, B. Q. Su and H. Shi, *Synth. React. Inorg. M.*, **47**, 396 (2016).
10. C. Haw, S. A. Rahman, W. Chiu, P. Khiew, S. Radiman, R. A. Shukor, M. A. A. Hamid and N. Ghazali, *New J. Chem.*, **40**, 1124 (2016).
11. G. V. Samsonov, N. F. Podgrushko, M. I. Lesnaya, L. A. Dvorina and N. F. Selivanova, *Sov. Phys. J.*, **18**, 1276 (1975).
12. K. A. Barrios, *J. Mater. Sci. Lett.*, **17**, 1095 (1998).
13. D. Das, H. K. Mishra, K. M. Parida and A. K. Dalai, *J. Mol. Catal. A-Chem.*, **189**, 271 (2002).
14. M. C. Tsai, P. H. Cheng, M. H. Lee, H. C. Lin and M. J. Chen, *J. Phys. D Appl. Phys.*, **49**, 265108 (2016).
15. I. M. A. Mohamed, V. D. Dao, N. A. M. Barakat, A. S. Yasin, A. Yousef and H.-S. Choi, *J. Colloid Interface Sci.*, **476**, 9 (2016).
16. L. J. Tomar, P. J. Bhatt, R. k. Desai and B. S. Chakrabarty, *JNAM*, **2**, 27 (2014).
17. J. Q. Zhang, L. Li, Z. X. Xiao, D. Liu, S. Wang, J. J. Zhang, Y. T. Hao and W. Z. Zhang, *Acs Sustain. Chem. Eng.*, **4**, 2037 (2016).
18. B. H. Yao, X. P. Han, Y. Lü, C. Peng and C. J. Zhang, *Mater. Sci. Forum*, **852**, 257 (2016).
19. J. Zhang, L. Li, J. Zhang, X. Zhang and W. Zhang, *New J. Chem.*, **41**, 9113 (2017).
20. R. A. Lucky, R. Sui, J. M. H. Lo and P. A. Charpentier, *Cryst. Growth Des.*, **10**, 1598 (2010).
21. A. A. Rodríguez-Rodríguez, S. Martínez-Montemayor, C. C. Leyva-Porras, F. E. Longoria-Rodríguez, E. Martínez-Guerra and M. Sánchez-Domínguez, *J. Nanomater.*, 2367856 (2017).
22. C. Y. Haw, W. S. Chiu, S. Abdul Rahman, P. Khiew, S. Radiman, R. Abd-Shukor, M. A. Hamid and N. Ghazali, *New J. Chem.*, **40**, 1124 (2015).
23. X. Gao, X. Liu, Z. Zhu, X. J. Wang and Z. Xie, *Sci. Rep-UK*, **6**, 30543 (2016).
24. S. Rana, J. Rawat and R. D. K. Misra, *Acta Biomater.*, **1**, 691 (2005).
25. K. Laohhasurayotin, S Pookboonmee, D. Viboonratanasri and W. Kangwansupamonkon, *Mater. Res. Bull.*, **47**, 1500 (2012).
26. Z. Yang, B. Wang and Y. Shi, *Appl. Surf. Sci.*, **399**, 192 (2017).
27. K. Panwar, M. Jassal and A. Agrawal, *Rsc Adv.*, **6**, 92754 (2016).
28. T. Čižmar, U. L. Štangar and I. Arčon, *Catal. Today*, **287**, 155 (2017).
29. M. V. Limaye, S. B. Singh, R. Das, P. Poddar, M. K. Abyaneh and S. K. Kulkarni, *J. Magn. Magn. Mater.*, **441**, 683 (2017).
30. D. Wang, J. Yang, X. Li, J. Wang, H. Zhai, J. Lang and H. Song, *Phys. Status. Solidi. A.*, **214**, 1600665 (2017).
31. M. O. Ojemaye, A. I. Okoh and O. O. Okoh, *J. Nanomater.*, **1**, 5264910 (2017).
32. D. Beydoun and R. Amal, *Mater. Sci. Eng. B-ADV*, **94**, 71 (2002).
33. Z. Li, Y. Yao, Y. Zheng, T. Gao, Z. Liu and G. Zhou, *J. Electrochem. Soc.*, **165**, 58 (2018).
34. M. Alijani, B. K. Kaleji and S. Rezaee, *J. Mater. Sci.-Mater. El.*, **28**, 15345 (2017).
35. D. Greene, R. Serrano-Garcia, J. Govan and Y. Gun'ko, *Nanomaterials-Basel*, **4**, 331 (2014).
36. H. Zhuang, Y. Zhang, Z. Chu, J. Long, X. An, H. Zhang and X. Wang, *Phys. Chem. Chem. Phys.*, **18**, 9636 (2016).
37. C. C. Chen, D. Jaihindh, S. H. Hu and Y. P. Fu, *J. Photoch. Photobio. A.*, **334**, 74 (2017).
38. M. A. Golsefidi and B. Sarkhosh, *J. Iran. Chem. Soc.*, **14**, 1089 (2017).
39. M. Xing, J. Zhang, B. Qiu, B. Tian, M. Anpo and M. Che, *Small*, **11**, 1920 (2015).
40. M. R. D. Khaki, M. S. Shafeeyan, A. A. A. Raman and W. M. A. W.

Daud, *J. Mater. Sci.-Mater. El.*, **29**, 5480 (2018).
41. M. Y. Xing, Y. Zhou, C. Y. Dong, L. J. Cai, L. X. Zeng, B. Shen, L. H. Pan, C. C. Dong, Y. Chai, J. L. Zhang and Y. D. Yin, *Nano Lett.*, **18**, 3384 (2018).
42. Z. Noorimotlagh, I. Kazeminezhad, N. Jaafarzadeh, M. Ahmadi, Z. Ramezani and S. Silva Martinez, *J. Hazard. Mater.*, **350**, 108 (2018).
43. J. J. Zhang, P. Qi, J. Li, X. C. Zheng, P. Liu, X. X. Guan and G. P. Zheng, *J. Ind. Eng. Chem.*, **61**, 407 (2018).
44. O. S. Ayanda, S. M. Nelana, L. F. Petrik and E. B. Naidoo, *J. Water Health*, **15**, 1015 (2017).